

Ground-based Multiwavelength Observations of Comet 103P/Hartley 2

A. Gicquel^{1,2}, S. N. Milam², G. L. Villanueva^{1,2}, A. J. Remijan³, I. M. Coulson⁴, Y.-L. Chuang⁵, S. B. Charnley², M. A. Cordiner^{1,2} and Y.-J. Kuan^{5,6}

ABSTRACT

The Jupiter-family comet 103P/Hartley 2 (103P) was the target of the NASA EPOXI mission. In support of this mission, we conducted observations from radio to submillimeter wavelengths of comet 103P in the three weeks preceding the spacecraft rendezvous on UT 2010 November 4.58. This time period included the passage at perihelion and the closest approach of the comet to the Earth. Here we report detections of HCN, H₂CO, CS, and OH and upper limits for HNC and DCN towards 103P, using the Arizona Radio Observatory Kitt Peak 12m telescope (ARO 12m) and submillimeter telescope (SMT), the James Clerk Maxwell Telescope (JCMT) and the Greenbank Telescope (GBT). The water production rate, $Q_{H_2O} = (0.67 - 1.07) \times 10^{28} \text{ s}^{-1}$, was determined from the GBT OH data. From the average abundance ratios of HCN and H₂CO relative to water ($0.13 \pm 0.03 \%$ and $0.14 \pm 0.03 \%$, respectively), we conclude that H₂CO is depleted and HCN is normal with respect to typically-observed cometary mixing ratios. However, the abundance ratio of HCN with water shows a large diversity with time. Using the JCMT data we measured an upper limit for the DCN/HCN ratio < 0.01 . Consecutive observations of *ortho*-H₂CO and *para*-H₂CO on November 2 (from data obtained at the JCMT), allowed us to derive an *ortho* : *para* ratio (OPR) $\approx 2.12 \pm 0.59 (1\sigma)$, corresponding to $T_{spin} > 8 \text{ K} (2\sigma)$.

Subject headings: Astrobiology – Comets: individual (103P/Hartley 2) – techniques: spectroscopic – radio lines: planetary systems – submillimeter lines: planetary systems

1. Introduction

Comets are probably the least-altered bodies in the Solar System (Festou et al. 2004). As

such, they can provide key insights into physical and chemical processes occurring during its origin and earliest evolutionary epochs, including the origin of long-period and short period comets (Duncan et al. 2004) and the formation and composition of planets (Dodson-Robinson et al. 2009; Bast et al. 2013). By studying comets from different reservoirs we can probe the different environments in which they formed and also better understand their role in initiating prebiotic chemistry on the early Earth through delivery of water and organic matter by cometary impacts (Chyba et al. 1990). Comets are primarily located in two distinct reservoirs of the Solar System: the Oort Cloud and the Kuiper Belt. The Oort Cloud is a source of long-period comets and (probably) Halley-type comets (Levison et al. 2001). The Kuiper Belt is a source of Jupiter family comets (Duncan et al. 2004;

¹Catholic University of America, Physics Department, 620 Michigan ave NE, Washington, DC;

²Goddard Center for Astrobiology, NASA Goddard Space Flight Center, 8800 Greenbelt Rd., Greenbelt, MD 20771, USA; adeline.gicquel@nasa.gov, stefanie.n.milam@nasa.gov, geronimo.l.villanueva@nasa.gov, steven.b.charnley@nasa.gov, martin.a.cordiner@nasa.gov.

³National Radio Astronomy Observatory, 520 Edge-mont Road, Charlottesville, VA 22903, USA; aremijan@nrao.edu.

⁴Joint Astronomy Centre, 660 N. A’ohoku Place University Park, Hilo, Hawaii 96720, USA; i.coulson@jach.hawaii.edu

⁵National Taiwan Normal University, 88 Sec. 4 Ting-Chou Rd., Taipei 116, Taiwan; ylchuang@std.ntnu.edu.tw

⁶Academia Sinica Institute of Astronomy & Astrophysics (ASIAA), Taipei 106, Taiwan; kuan@ntnu.edu.tw

Levison & Duncan 1997). To explore the connections among the formation environment, subsequent chemical evolution, and present composition of comets, efforts have been made to develop chemical taxonomies (A’Hearn et al. 1995; Bockelée-Morvan et al. 2004; Bockelée-Morvan & de Bergh 2005; Feldman et al. 2005; Crovisier et al. 2009; Fink 2009; Mumma & Charnley 2011). Important cosmogonic quantities for the investigation of primordial constitutions (such as the *ortho* : *para* and D/H ratios), can be obtained by observations of comets from ground-based, space-based and airborne observatories (Crovisier et al. 1997; Biver et al. 2007; Hartogh et al. 2011; Reach et al. 2013; Hines et al. 2014), as well as from laboratory analyses of cometary (interplanetary) dust particles collected in the stratosphere (Starkey & Franchi 2013). These data provide measurements of chemical composition, isotopic ratios and molecular spin ratios, which are important to help establish the contribution of the Solar System’s natal molecular cloud to the compositions of primitive materials and comets. In addition, isotopic ratios such as D/H can be compared with the value for the Earth’s ocean water to investigate the possible importance of cometary water delivery.

Comet rendezvous space missions to individual comets present unique scientific opportunities. *In situ* spacecraft observations of several comets have allowed their nuclei to be imaged and the gas and dust properties of their comae to be studied in great detail. These include: 1P/Halley (Newburn et al. 1991); 81P/Wild 2 (Brownlee et al. 2006); 9P/Tempel (A’Hearn et al. 2005); 103P/Hartley 2 (A’Hearn et al. 2011); and the current ROSETTA mission to 67P/Churyumov-Gerasimenko (Schulz 2012). Ground-based observing campaigns have also played an important role in support of space missions (Meech et al. 2005, 2011; Knight et al. 2007) and, in the case of 81P/Wild 2, laboratory analyses of the returned Stardust samples have yielded unique insights into the nature of cometary dust (McKeegan et al. 2006; Clemett et al. 2010).

Comet 103P/Hartley 2 (hereafter 103P) is a Jupiter-family comet, with a short orbital period (6.5 years), and a low orbital inclination. It was the target of the NASA EPOXI mission (A’Hearn et al. 2011; Meech et al. 2011). The comet passed perihelion on 2010 October 28 at

$R_h = 1.059$ AU and on 2010 October 21 made an exceptionally close approach to Earth at $\Delta = 0.12$ AU. In support of the EPOXI mission, we conducted observations at radio and submillimeter wavelengths of comet 103P in the three weeks preceding the spacecraft rendezvous on UT 2010 November 4.58. Here we report detections of HCN, H₂CO, CS, and OH and upper limits for HNC and DCN, using the 12m Arizona Radio Observatory Kitt Peak (12m) and the 10m submillimeter telescope (SMT), as well as the 15m James Clerk Maxwell Telescope (JCMT) and the 100m Robert C. Byrd Greenbank Telescope (GBT). We present the observational results and determine physical parameters such as column densities, and production rates. Finally, the *ortho* : *para* ratio has been derived from H₂CO, and an upper limit on the D/H ratio was obtained from DCN and HCN measurements.

2. Observations

Comet 103P/Hartley 2 was discovered on 1984 June 4 by Malcolm Hartley at the Siding Spring Observatory (Hartley 1986). 103P has been frequently observed over the 30 years following its discovery, both by ground-based and space telescopes. Observations provided information about the gas production rate (A’Hearn et al. 1995; Crovisier et al. 1999; Colangeli et al. 1999; Fink 2009; Combi et al. 2011), and the mean radius (Lisse et al. 2009). All the observations presented here adopted the same JPL/Horizons (Jet Propulsion Laboratory) ephemeris number 183.

2.1. Green Bank Telescope (GBT)

Observations of comet 103P were made between 2010 October 13 and October 31 for monitoring emission from the OH: J = 3/2, $\Omega=3/2$, F=1⁺-1⁻ (1667.3 MHz/18 cm) lines at L-band (Program ID GBT/10C-059). A barycentric velocity reference frame was assumed for all observations. The line of sight radial velocity on each day recorded by the JPL ephemeris was then subtracted from the data to set each spectral feature to a 0 km s⁻¹ cometocentric velocity. The GBT spectrometer was configured in its eight intermediate-frequency (IF), 12.5 MHz three-level mode, which enabled observing four 12.5 MHz frequency bands simultaneously in two polarizations through the use of offset os-

cillators in the IF. Antenna temperatures were recorded on the T_A^* scale (Ulich & Haas 1976) with estimated 20% uncertainties. Data were taken in the OFF-ON position-switching mode, with the OFF position 60' east in azimuth with respect to the ON-source position. A single scan consisted of 2 minutes in the OFF-source position followed by 2 minutes in the ON-source position. Automatically-updated dynamic pointing corrections were employed based on real-time temperature measurements of the structure input to a thermal model of the GBT. Zero points were adjusted at the beginning of each observing run by pointing on a nearby quasar. The pointing accuracy of the GBT is 5" (rms) for blind pointing and 7" (rms) for offset pointing. The GBT beam size at this frequency is $\approx 8'$.

2.2. Arizona Radio Observatory 12m (12m) and Submillimeter Telescope (SMT)

Observations of HCN: J = 3-2 (265.8864 GHz), *o*-H₂CO: $J_{K_a, K_c} = 3_{1,2}-2_{1,1}$ (225.6978GHz), HCN: J = 1-0 (88.6318GHz), HCN: J = 2-1 (177.2612GHz), and CS: J = 4-3 (97.9809GHz), toward comet 103P were taken between 2010 October 22 and November 4 using the facilities of the Arizona Radio Observatory (ARO): the 12m telescope on Kitt Peak, Arizona and the SMT on Mount Graham, Arizona. The 1 mm observations were carried out at the SMT with a dual-polarization ALMA Band 6 receiver system, employing sideband-separating mixers with an image rejection of typically 15–20 dB. The backends employed were a 2048 channel 1 MHz filter bank used in parallel (2×1024) mode, and 250 kHz filter also in parallel (2×250). The temperature scale at the SMT is T_A^* ; radiation temperature is then defined as $T_R = T_A^*/\eta_b$, where η_b is the main beam efficiency. The 2 and 3mm observations were conducted at the ARO 12 m using dual-polarization SIS mixers, operated in single-sideband mode with the image rejection ≥ 20 dB. Filter banks with 512 channels of 100 and 250 KHz resolutions were used simultaneously in parallel mode for the measurements, along with an autocorrelator with 782 kHz resolution. The intensity scale of the 12 m is the chopper-wheel corrected antenna temperature, T_R^* , including forward spillover losses, which is converted to radiation temperature by $T_R = T_R^*/\eta_c$, where η_c is the

corrected beam efficiency. Data at both facilities were taken in position-switching mode with an off position 30' west in azimuth. The JPL ephemeris was used to determine the cometary position using the orbital elements. The pointing accuracy is estimated at 1" rms for the SMT and 5" for the ARO 12m. Focus and positional accuracy were checked periodically on nearby planets or masers.

2.3. James Clerk Maxwell Telescope (JCMT)

Sub-millimeter spectroscopic observations of 103P (Programme ID m10bu13) were made from the JCMT, located at the 4000m level on Mauna Kea, Hawaii, on UT 2010 October 21, 22, 23, 25 and November 02, 03, 04, using the HARP heterodyne array. HARP is a 4×4 array receiver, but was used here in a single-receptor mode. HARP is remotely and quickly tunable to frequencies in the 325-375GHz ranges and utilizes an image sideband suppressor. The output from the HARP receiver is fed to the 'ACSIS' digital autocorrelation spectrometer. For this work, ACSIS was configured at its highest frequency resolutions (31MHz). Observations of HCN: J = 4-3 (354.5055GHz), HCN: J = 3-2 (265.8864GHz), *p*-H₂CO: $J_{K_a, K_c} = 5_{0,5}-4_{0,4}$ (362.7360GHz), *o*-H₂CO: $J_{K_a, K_c} = 5_{1,5}-4_{1,4}$ (351.7686GHz), DCN: J = 5-4 (362.0465GHz) and HNC: J = 4-3 (362.6303GHz) were measured at the JCMT.

At these frequencies, the JCMT has a Gaussian beam of size $\approx 15''$ (full width at half power). The HARP receptors are separated by about $30''$, and so the emission from the comet is anticipated to be encompassed by a single receptor – the 'pointing' receptor. Pointing of the telescope is achieved by doing spectral-line 'five-points' on nearby line sources, and pointing accuracy is estimated at 2" rms in each of two orthogonal coordinates (azimuth and elevation). A pointing check was performed approximately every hour. Telescope focus is similarly maintained throughout the night by measures of bright line-sources. Calibration of the (T_A^*) brightness scale is achieved by making measures at standard frequencies (eg CO: J = 3-2, 345GHz) of astronomical sources used as reference calibrators.

The opacity of the sky above JCMT was measured by a water vapor meter (WVM) mounted so as to measure along the telescope line-of-sight. Opacity is expressed as if measured at the zenith

at 225GHz. The opacity (in nepers) on UT Oct 21, 22, 23, 25 was, on average, 0.10, 0.05, 0.05, 0.05 and on Nov 02, 03, 04 was 0.09, 0.11, 0.15. The latter conditions made observations difficult at these HARP (B-band) frequencies, but conditions otherwise were most suitable for this program.

3. Results

Observed lines parameters including UT dates, observing frequencies (ν), beam size (Θ_b), diameter of the projected beam size on the comet (D), beam efficiency (η_c or η_b), temperature (T_R^* or T_A^*), FWHM line width ($\Delta v_{1/2}$), integrated intensity ($\int T_R^* \Delta v_{1/2}$), heliocentric distance (R_h) and comet distance at the times of measurements (Δ) are listed in Table 1. The uncertainties of the line width and the integrated line intensity are determined from a Gaussian fit and are reported at 1σ in the Table 1.

Representative spectra are shown in Figures 1 – 4 from all facilities. All the spectra are plotted in the cometocentric velocity frame. The UT date of each observed transition is located in the Figure. All data are included as supplemental information.

Figure 1 displays the OH detection toward comet 103P/Hartley 2 from the GBT taken on 2010 October 13 and 19. The GBT data were measured in a monitoring sequence every 1, 2, 3 or 5 days. The OH line inversion and gas production rates on these days are reported in Table 2.

Figure 2 displays the $J = 4-3$ and the $J = 3-2$ transitions of HNC on 2010 October 22 toward comet 103P/Hartley 2 from the JCMT and SMT, respectively. We detected four transitions of HCN with three telescopes (SMT, 12m and JCMT). Gas production rates from these transition are reported in Table 3. Figure 2 shows two transitions observed on the same day. Furthermore, the line is mostly resolved with the JCMT and partially with the SMT.

Figure 3 displays the $J = 2-1$ transitions of CS on 2010 October 22 toward comet 103P/Hartley 2 from the 12m. Gas production rates from this transition are reported in Table 3. These data were collected with a resolution of $\approx 0.310 \text{ km s}^{-1}$ and show a narrow line width. The line profile is not resolved here and only provides details on abundance and not molecular origin within the

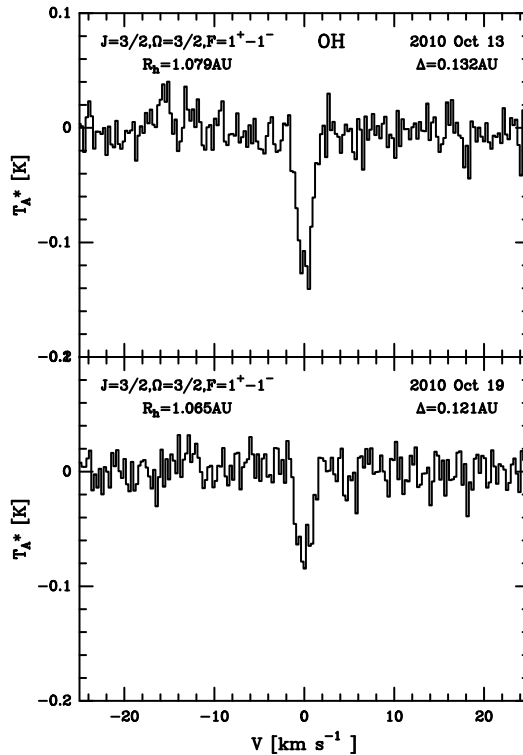


Fig. 1.— Detection of OH taken on 2010 October 13 and 19 with the GBT. The spectral resolution is $\approx 0.274 \text{ km s}^{-1}$. Additional spectra from the observing campaign for OH is available in Appendix A.

coma.

Figure 4 displays respectively the $J_{K_a, K_c} = 5_{0,5}-4_{0,4}$ and $J_{K_a, K_c} = 5_{1,5}-4_{1,4}$ transitions of *p*-H₂CO and *o*-H₂CO on 2010 November 2 toward comet 103P/Hartley 2 from the JCMT. We observed *p*-H₂CO and *o*-H₂CO the same day only with the JCMT. A detailed discussion on the *ortho* : *para* ratio can be found in section 4.4.

4. Analysis

4.1. Column densities, Production rates and Abundances

The production rate for water was indirectly measured from the observation of its photodissociation product OH with the GBT. We used the equation of Tacconi-Garman et al. (1990) to determine the total OH production rate (Q_{OH}) for each observation:

TABLE 1
OBSERVATIONS OF OH, HCN, H₂CO, CS, DCN AND HNC WITH THE GBT, JCMT, SMT AND 12M
TOWARD COMET 103P/HARTLEY 2. A. T_R^* AND η_c FOR THE 12M, T_A^* AND η_b FOR THE SMT, JCMT
AND GBT.

Line	Telescope	Transition	UT Date	ν (MHz)	Θ_b (")	D (km)	η_c or η_b^A	T_R^* or T_A^* (K)	$\Delta v_{1/2}$ (km s ⁻¹)	$\int T_R^* \Delta v_{1/2}$ (K km s ⁻¹)	R _h (AU)	Δ (AU)	
OH	GBT	multiple lines	2010 Oct 13.04	1667.3	452.8	43348	0.95	-0.13 ± 0.01	1.84 ± 0.13	-0.24 ± 0.02	1.079	0.132	
			2010 Oct 15.04					41706	-0.14 ± 0.01	2.05 ± 0.14	-0.28 ± 0.02	1.074	0.127
			2010 Oct 16.40					40721	-0.10 ± 0.01	1.74 ± 0.15	-0.18 ± 0.03	1.071	0.124
			2010 Oct 19.44					39736	-0.07 ± 0.01	1.65 ± 0.21	-0.12 ± 0.02	1.065	0.121
			2010 Oct 22.31					39736	-0.03 ± 0.01	2.09 ± 0.28	< -0.07	1.062	0.121
			2010 Oct 23.46					40064	-0.04 ± 0.01	1.85 ± 0.39	< -0.07	1.061	0.122
			2010 Oct 24.46					40393	-0.03 ± 0.01	1.08 ± 0.32	< -0.03	1.060	0.123
			2010 Oct 26.44					41706	0.01 ± 0.01	1.86 ± 0.75	< 0.03	1.059	0.127
			2010 Oct 28.18					43020	0.03 ± 0.01	1.44 ± 0.34	< 0.04	1.059	0.131
			2010 Oct 31.57					46304	0.03 ± 0.01	2.29 ± 0.79	< 0.07	1.060	0.141
			2010 Oct 22.54					2492	0.24 ± 0.01	1.20 ± 0.30	0.23 ± 0.03	1.062	0.121
			2010 Oct 29.35					2750	0.19 ± 0.05	1.06 ± 0.30	0.21 ± 0.01	1.059	0.134
2010 Nov 1.32	2955	0.14 ± 0.03	1.17 ± 0.10	0.16 ± 0.03	1.060	0.144							
2010 Nov 1.68	2976	0.30 ± 0.04	1.21 ± 0.10	0.36 ± 0.04	1.060	0.144							
2010 Nov 4.65	3212	0.37 ± 0.01	1.40 ± 0.30	0.38 ± 0.03	1.063	0.156							
o-H ₂ CO	SMT	3 _{1,2} - 2 _{1,1}	2010 Oct 29.55	225697.8	33.3	3264	0.95	0.01 ± 0.03	1.96 ± 0.30	0.03 ± 0.01	1.059	0.134	
HCN	12m	1-0	2010 Oct 22.31	88631.8	70.7	6208	0.95	0.05 ± 0.01	1.50 ± 0.30	0.07 ± 0.01	1.062	0.121	
			2010 Oct 23.33			6260	0.08 ± 0.02	0.50 ± 0.20	0.04 ± 0.01	1.061	0.122		
2010 Oct 24.31	6311	0.07 ± 0.02	0.90 ± 0.20	0.07 ± 0.01	1.060	0.123							
2010 Oct 28.3	6732	0.05 ± 0.03	1.62 ± 0.30	0.08 ± 0.05	1.059	0.131							
HCN	12m	2-1	2010 Oct 23.54	177261.2	35.4	3130	0.65	0.35 ± 0.02	1.00 ± 0.40	0.34 ± 0.07	1.061	0.122	
CS	12m	2-1	2010 Oct 22.53	97980.9	64.0	5616	0.88	0.07 ± 0.02	0.40 ± 0.20	0.03 ± 0.01	1.062	0.121	
HCN	JCMT	4-3	2010 Oct 21.48	354505.5	14.1	1242	0.63	0.61 ± 0.03	1.16 ± 0.06	0.75 ± 0.05	1.063	0.121	
			2010 Oct 22.43			1242	0.59 ± 0.06	1.20 ± 0.20	0.79 ± 0.13	1.062	0.121		
			2010 Oct 22.78			1252	0.97 ± 0.08	1.30 ± 0.20	1.31 ± 0.17	1.061	0.122		
			2010 Oct 23.41			1252	0.57 ± 0.04	1.20 ± 0.10	0.73 ± 0.07	1.061	0.122		
			2010 Oct 23.77			1262	0.55 ± 0.04	1.20 ± 0.10	0.67 ± 0.08	1.061	0.123		
			2010 Nov 2.44			1519	0.79 ± 0.05	1.20 ± 0.10	1.03 ± 0.10	1.061	0.148		
			2010 Nov 2.77			1529	0.37 ± 0.05	1.40 ± 0.20	0.55 ± 0.11	1.061	0.149		
			2010 Nov 3.62			1560	0.30 ± 0.04	1.10 ± 0.20	0.33 ± 0.07	1.062	0.152		
			2010 Nov 4.44			1601	0.48 ± 0.05	1.30 ± 0.20	0.67 ± 0.11	1.063	0.156		
			2010 Oct 25.56			1716	0.33 ± 0.05	1.20 ± 0.20	0.42 ± 0.09	1.059	0.125		
			2010 Oct 21.56			1214	0.31 ± 0.01	0.03 ± 0.50	0.008 ± 0.002	1.063	0.121		
			2010 Oct 23.57			1234	0.04 ± 0.01	0.39 ± 0.12	0.016 ± 0.007	1.061	0.123		
			2010 Nov 2.69			1494	0.05 ± 0.08	1.00 ± 0.50	0.049 ± 0.008	1.061	0.149		
			2010 Nov 2.58			1531	0.05 ± 0.01	1.60 ± 0.30	0.079 ± 0.018	1.061	0.148		
			2010 Oct 22.58			1216	-	-	< 0.01	1.062	0.121		
			2010 Oct 23.57			1236	-	-	< 0.01	1.061	0.123		
2010 Nov 2.69	1497	-	-	< 0.03	1.061	0.149							
2010 Nov 4.67	1568	-	-	< 0.04	1.063	0.156							
2010 Nov 2.69	1495	-	-	< 0.03	1.061	0.149							
2010 Nov 4.67	1565	-	-	< 0.04	1.063	0.156							

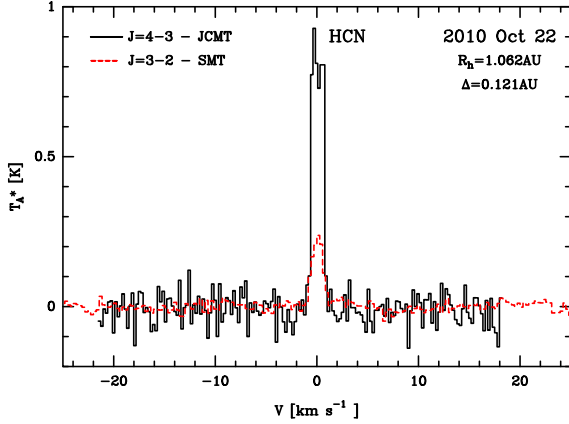


Fig. 2.— Detection of HCN taken on 2010 October 22 with the JCMT (dark solid line) and the SMT (red dashed line). The spectral resolution are $\approx 0.232 \text{ km s}^{-1}$ and $\approx 0.280 \text{ km s}^{-1}$ for the JCMT and the SMT, respectively. (For interpretation of the references to color in this Figure legend, the reader is referred to the web version of this article.). The detections of HCN from all facilities and dates are available in Appendix B.

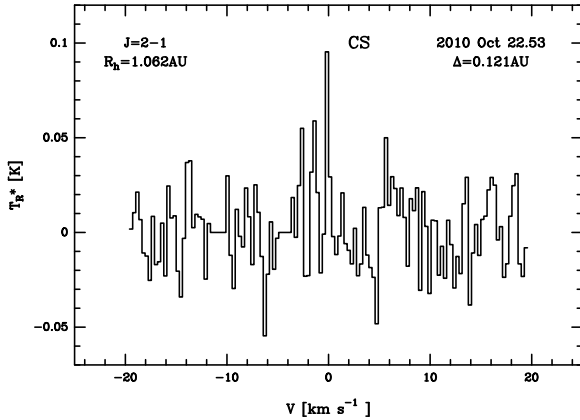


Fig. 3.— Detection of CS 2-1 taken on 2010 October 22 with the 12m. The spectral resolution is $\approx 0.310 \text{ km s}^{-1}$.

$$Q_{OH} = \left(\frac{7.06 \times 10^{25}}{i} \right) \left(\frac{3.3}{T_{BG}} \right) \left(\frac{10^5}{\tau_{OH}} \right) \left(\frac{\Delta}{1} \right)^2 \left(\frac{I_{OH}}{1} \right) \quad (1)$$

where i is the inversion of the ground state, T_{BG} (K) is the background temperature, τ_{OH} (s) is the lifetime of the OH molecule, Δ (AU) is the Earth-comet distance and I_{OH} (mJy km s^{-1}) is the inte-

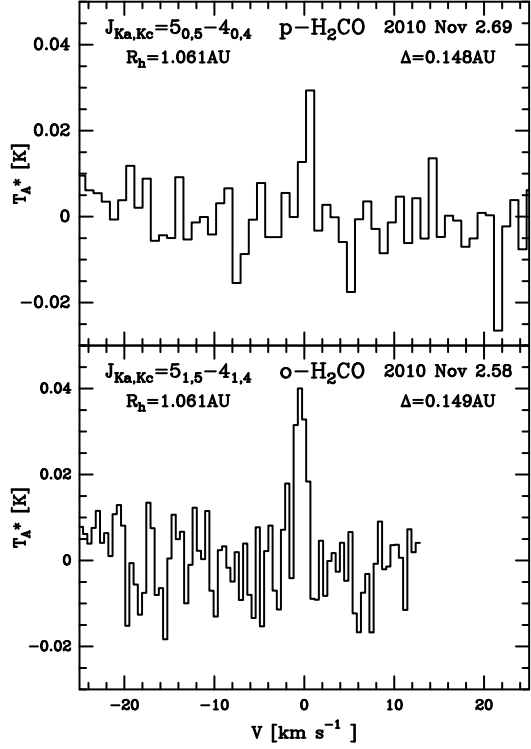


Fig. 4.— Detection of H₂CO taken on 2010 November 2 with the JCMT. The spectral resolution are $\approx 0.909 \text{ km s}^{-1}$ and $\approx 0.468 \text{ km s}^{-1}$ for $p\text{-H}_2\text{CO}$ and $o\text{-H}_2\text{CO}$, respectively. The detection of H₂CO from all facilities and dates are available in Appendix C.

grated flux. The dominant source of error in this formalism comes from the accuracy of the integrated flux measurement, as well as the inversion parameter i , although the latter is negligible for these data.

Given that the values of the heliocentric velocity (R_{dot}) of the comet ranged from -5 to +2 (Table 2), a polynomial function was fit to the data presented in Table 5 of Schleicher & A'Hearn (1988) between these values in order to find the inversion at the comet's heliocentric velocity on the date and UT time of the observations. This inversion value is given in Table 2. The OH photodissociation lifetime (τ_{OH}) is $1.2 \times 10^5 R_h^2 \text{ s}$ (taken from Tacconi-Garman et al. 1990), and is used in the final production rate calculation, and we assume $T_{BG} = 2.7 \text{ K}$. The measured intensity and line width of each transition is given in Table 1. The

Q_{OH} value is then corrected by a factor P , which is defined as the fraction of molecules in the coma that are contained within the GBT beam. We computed P using a Monte-Carlo Haser model (Haser 1957) for daughter molecules, assuming $\tau_{H_2O} = 8.0 \times 10^4 R_h^2$ (s) (Huebner et al. 1992), $v_{OH} = 0.95 \text{ km s}^{-1}$ and $v_{H_2O} = 0.80 \text{ km s}^{-1}$ (Crovisier et al. 2013). The final production rates for OH on each date are given in Table 2. Q_{OH} shows large diversity with time. The average measured production rate of OH over this monitoring campaign is $Q_{OH} = (7.03 \pm 0.44) \times 10^{27} \text{ s}^{-1}$. The conversion to Q_{H_2O} is made by dividing the Q_{OH} by the branching ratio of water dissociation to OH. The photodissociation of the H_2O molecule into H and OH is the most important process accounting for 85.5% of all water molecules that are dissociated (Harris et al. 2002). The mean water production rate was therefore $Q_{H_2O} = (8.22 \pm 0.51) \times 10^{27} \text{ s}^{-1}$.

Water production was directly measured in this comet from submillimeter rotational transitions from space with Odin (Biver et al. 2011), with the three instruments of Herschel (Lis et al. 2010; Hartogh et al. 2011; Meech et al. 2011), and from rovibrational lines in the infrared from the ground (Dello Russo et al. 2011; Mumma et al. 2011). It was indirectly measured from the observation of its photodissociation products: of OH in the near-UV (Knight & Schleicher 2012), of H from the Ly $-\alpha$ line observed by SOHO/SWAN (Combi et al. 2011) and of OH at 18 cm (here and Crovisier et al. 2013). Published water production rates from concurrent observations within ± 50 days of perihelion (labeled as Jr) ranged from 0.1 to $1.9 \times 10^{28} \text{ s}^{-1}$ and are summarized in Figure 5. The values from this work are consistent with the value derived by Mumma et al. (2011) and Combi et al. (2011). The observed variation in Q_{H_2O} as been attributed to the rotation of the nucleus (Mumma et al. 2011; Biver et al. 2011).

Beam-averaged column densities were derived for HCN, H_2CO , CS, DCN and HNC assuming that the cometary coma filled the beams of the respective telescopes. In the case of the upper limits, a 3σ rms was assumed to derive the integrated intensity of DCN and HNC, set at the linewidth of $\approx 1 \text{ km s}^{-1}$. The column density for the observa-

tions was calculated from:

$$N_{tot} = \frac{8\pi k\nu^2 \int T_R \Delta v_{1/2} \zeta_{rot} e^{E_{up}/kT_{rot}}}{hc^3 A_{ul} g_{up} \eta c}, \quad (2)$$

where k is the Boltzmann constant, ζ_{rot} is the partition function, h is the Planck constant, c is the speed of the light, A_{ul} [s^{-1}] is the Einstein coefficient, g_{up} is the statistical weight, T_{rot} [K] is the rotational excitation temperature, E_{up} [cm^{-1}] is the upper state energy, and N_{tot} [cm^{-2}] is the total number of molecules observed in the beam. Drahus et al. (2012) concluded that the rotational temperature from CH_3OH (157.225 GHz; IRAM 30m telescope) varied strongly, due to the nucleus rotation, with the average value being 47 K (between 19-179 K). Additionally, Boissier et al. (2014) derived T_{rot} from CH_3OH (157.225 GHz; IRAM 30m telescope and the Plateau de Bure) as a function of the radii of the projected beam sizes on the coma. They concluded that the increase of T_{rot} from $\approx 35\text{K}$ to $\approx 46 \text{ K}$ is due to the increase of the beam radii from $\approx 150 \text{ km}$ to $\approx 1500 \text{ km}$. In this analysis, we assumed $T_{rot} = 50 \text{ K}$, which is the average from CH_3OH observations conducted at the same facilities during our observations (Chuang et al. 2014, in preparation). This is consistent with other results considering a diameter of the projected beam sizes on the coma between $\approx 1200 \text{ km}$ to $\approx 46,400 \text{ km}$ (Table 1). The column densities derived for HCN, H_2CO , CS, DCN and HNC are listed in Table 3. The minimum ($T_{rot} = 19\text{K}$) and maximum rotational ($T_{rot} = 179 \text{ K}$) temperatures obtained by Drahus et al. (2012) provide $N_{tot} = (6.29 \pm 0.34) \times 10^{11} \text{ cm}^{-2}$ and $N_{tot} = (2.32 \pm 0.12) \times 10^{11} \text{ cm}^{-2}$, respectively on 2010 October 22 for HCN: $J = 3 - 2$. The D/H and *ortho:para* ratio are discussed in sections 4.3 and 4.4, respectively.

Most of the molecular species measured are considered to be parent species, thus production rates were determined from a Monte Carlo model (Milam et al. 2004, 2006) that traces the trajectories of molecules within the telescope beam, ejected from the comet nucleus. The observed column density is then matched for an output molecular production rate, Q . H_2CO is considered as both a parent and extended source species, so production rates were derived for both cases employing the models of Milam et al. (2006). Table 3 summarizes the production rates of the molecules observed toward comet 103P, the production rate

Table 2: OH and H₂O production rates with the GBT toward comet 103P/Hartley 2.

Line	Telescope	UT Date	R_{dot} (km s ⁻¹)	i calculated	P	Q_{OH} (s ⁻¹)	Q_{H_2O} (s ⁻¹)
OH	GBT	2010 Oct 13.04	-4.99	-0.26	0.063	$(6.99 \pm 0.73) \times 10^{27}$	$(8.17 \pm 0.85) \times 10^{27}$
		2010 Oct 15.04	-4.11	-0.23	0.061	$(9.13 \pm 0.91) \times 10^{27}$	$(1.07 \pm 0.11) \times 10^{28}$
		2010 Oct 16.40	-3.70	-0.21	0.059	$(6.26 \pm 0.81) \times 10^{27}$	$(7.32 \pm 0.95) \times 10^{27}$
		2010 Oct 19.44	-2.89	-0.15	0.058	$(5.73 \pm 1.07) \times 10^{27}$	$(6.71 \pm 1.25) \times 10^{27}$

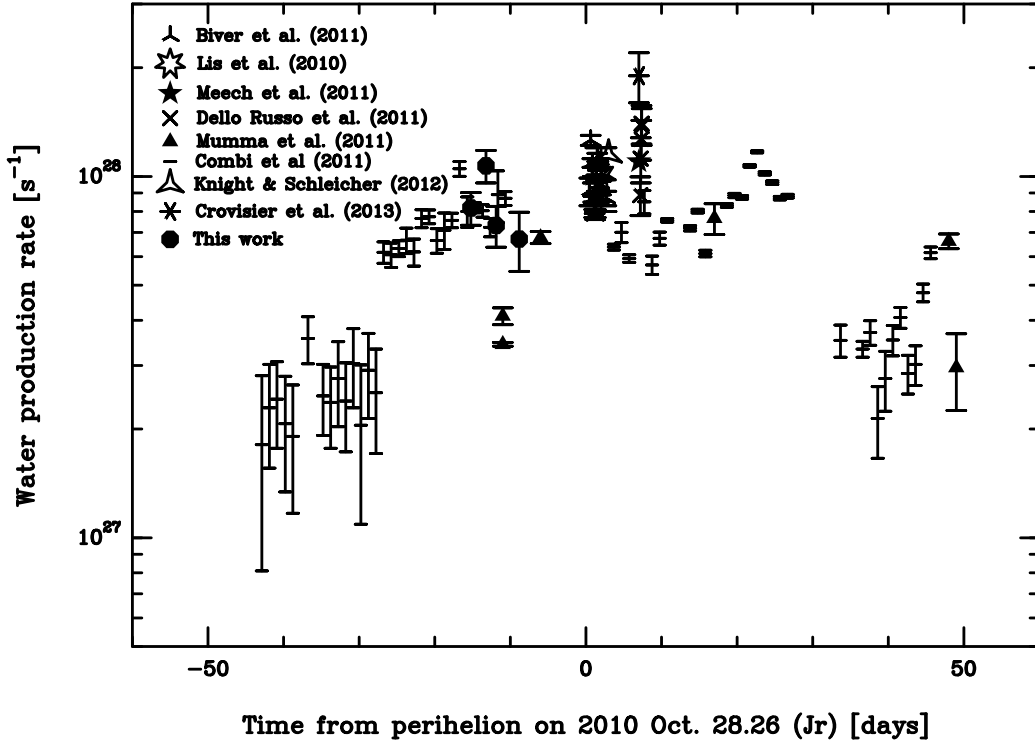


Fig. 5.— Water production rates measured in comet 103P/Harley 2 as a function of the time from perihelion on 2010 Oct. 28.26 (defined as Jr). Between Jr+1 and Jr+3 days, the observations are essentially from Biver et al. (2011) who studied the short-term variability of water. Lis et al. (2010) and Knight & Schleicher (2012), derived $Q_{H_2O} = (1.0 \pm 0.2) \times 10^{28} \text{ s}^{-1}$ and at Jr+3 and $Q_{H_2O} = 1.15 \times 10^{28} \text{ s}^{-1}$ at Jr+2 days, respectively. At Jr+7 days, the observations are essentially from Dello Russo et al. (2011). Meech et al. (2011) and Crovisier et al. (2013) derived $Q_{H_2O} = 1.2 \times 10^{28} \text{ s}^{-1}$ and $Q_{H_2O} = (1.9 \pm 0.3) \times 10^{28} \text{ s}^{-1}$, respectively.

of water and the ratio Q/Q_{H_2O} with the SMT, 12m, and JCMT. This model assumes isotropic outgassing, which is reasonable for the analysis of these data since the model simulates the observed column densities within a large beam (with respect to the comet). The uncertainties introduced into the modeled production rates are dominated by the errors on the measured column densities.

4.2. 103P/Hartley 2 previous measurements

Crovisier et al. (2013) observed the short-term variation of the OH production rate at Nancay in 2010 October. The production rate increased steeply and progressively before perihelion, reaching a maximum just before the EPOXI flyby. The water production rate preceding perihelion measured by SOHO/SWAN also shows an increase by a similar amount (Combi et al. 2011). By using the GBT data, one can also see that Q_{OH} increased as the comet was approaching the Sun (Appendix A). The time step of the GBT data cannot be used to correlate the temporal evolution of the water production rate with the rotational period of the comet, as studied with some other data, due to the long lifetime of OH and the large beam telescope beam. For example, Mumma et al. (2011) reproduced the temporal evolution of water with a cometary rotational period of 18 hours.

Mumma et al. (2011) also showed that the production rates for ethane, HCN, and methanol vary in a manner consistent with independent measures of nucleus rotation. Similar to OH, the time steps of our HCN observations were not adequate to study the short-term variability of HCN. Drahus et al. (2012) and Boissier et al. (2014) studied in detail the short-term variability of HCN. Drahus et al. (2012) observed a perfect phasing between the CH₃OH and HCN production rates. Boissier et al. (2014) compared the production curves of HCN, H₂O, CH₃OH, and CO₂. They showed that the curves of H₂O, CH₃OH and HCN are in phase, but there is a delay of ≈ 1.7 hrs with CO₂. They concluded that this delay can be due to the production of H₂O, CH₃OH, and HCN from subliming icy grains, whereas CO₂ molecules were released from the nucleus. By studying the spatial distribution of parent volatiles in comet 103P observed in the infrared, Kawakita et al.

(2013) reported that the spatial distributions of HCN, C₂H₂, C₂H₆ were extended in the anti-solar direction, while the spatial distributions of H₂O and CH₃OH were significantly extended in the solar direction. They also concluded that the molecules are produced from the sublimation of icy grains but that there might be two distinct phases of ice in 103P; one enriched in H₂O and CH₃OH, and another enriched in more volatile species (HCN, C₂H₂, C₂H₆). This asymmetry in the line profile mentioned by Kawakita et al. (2013) can be observed for HCN with the JCMT (Appendix B.).

In Table 3 we can see that the abundance ratio of HCN with water shows large variation with time, so the average is more representative of the global chemistry. This range can be explained by the asymmetric spatial profiles of the molecules (Kawakita et al. 2013), because the molecules are from different parts of the nucleus, or because of the sublimation of icy grains. The significant contribution of grain sublimation to the production of volatiles is supported by numerous measurements (A’Hearn et al. 2011; Mumma et al. 2011; Dello Russo et al. 2011; Drahus et al. 2012; Knight & Schleicher 2012). By averaging the abundance ratio of HCN and *o*-H₂CO with water, we obtain $Q(\text{HCN})/Q(\text{H}_2\text{O}) = 0.13 \pm 0.03$ % and $Q(\text{H}_2\text{CO})/Q(\text{H}_2\text{O}) = 0.14 \pm 0.03$ %. Boissier et al. (2014) derived an average abundance of HCN relative to water from millimeter observations consistent with our results. They detected HCN on 2010 October 23, November 4 and 5 with the IRAM interferometer located at the Plateau de Bure and obtained $Q(\text{HCN})/Q(\text{H}_2\text{O}) = 0.16$ %. The HCN abundances from millimeter observations were lower than the values from infrared data ($Q(\text{HCN})/Q(\text{H}_2\text{O}) \approx 0.3$ % Dello Russo et al. 2011, 2013; Mumma et al. 2011; Kawakita et al. 2013), by the typical factor of ≈ 2 (Villanueva et al. 2013). We deduced an average abundance of H₂CO relative to water in good agreement with Dello Russo et al. (2013) and Kawakita et al. (2013) $\approx 0.11\%$, but the value from this work is lower than the one from Mumma et al. (2011). The discrepancy between radio and IR results is not surprising given the strong temporal variability of the coma and differences in field of view. However, by comparison with other comets, we find the same approximate

TABLE 3

COLUMN DENSITIES, PHOTODISSOCIATION RATES, PRODUCTION RATES FOR HCN, H₂CO, CS, DCN AND HNC, PRODUCTION RATE OF WATER AND THE RATIO Q/Q_{H_2O} WITH THE SMT, 12M, AND JCMT. Q_{H_2O} ARE TAKEN FROM COMPARABLE DATE (FIGURE 5). THE PHOTODISSOCIATION RATES ARE FROM PHOTO IONIZATION/DISSOCIATION RATES. * DENOTES THE EPOXI FLYBY.

Line	Telescope	Transition	UT Date	N_{tot} (cm^{-2})	Rate (s^{-1})	Q (s^{-1})	Q/Q_{H_2O} (%)				
HCN	SMT	3-2	2010 Oct 22.54	$(2.72 \pm 0.38) \times 10^{11}$	1.31×10^{-05}	$(4.25 \pm 0.59) \times 10^{24}$	$(6.27 \pm 0.91) \times 10^{-02}$				
			2010 Oct 29.35	$(2.45 \pm 0.13) \times 10^{11}$		$(3.77 \pm 0.20) \times 10^{24}$	$(5.91 \pm 0.34) \times 10^{-02}$				
			2010 Nov 1.32	$(1.93 \pm 0.36) \times 10^{11}$		$(3.55 \pm 0.66) \times 10^{24}$	$(5.06 \pm 0.99) \times 10^{-02}$				
			2010 Nov 1.68	$(4.34 \pm 0.48) \times 10^{11}$		$(8.18 \pm 0.90) \times 10^{24}$	$(1.17 \pm 0.15) \times 10^{-01}$				
o-H ₂ CO	SMT	3 _{1,2} - 2 _{1,1}	2010 Oct 29.55	$(2.39 \pm 0.35) \times 10^{11}$	2.15×10^{-04}	$(1.07 \pm 0.16) \times 10^{25}$	$(1.68 \pm 0.25) \times 10^{-01}$				
			2010 Oct 22.31	$(3.94 \pm 0.67) \times 10^{11}$		$(1.97 \pm 0.34) \times 10^{25}$	$(2.91 \pm 0.51) \times 10^{-01}$				
			2010 Oct 23.33	$(2.33 \pm 0.78) \times 10^{11}$		$(4.38 \pm 1.45) \times 10^{24}$	$(6.45 \pm 2.17) \times 10^{-02}$				
			2010 Oct 24.31	$(3.68 \pm 0.67) \times 10^{11}$		$(1.17 \pm 0.22) \times 10^{25}$	$(1.73 \pm 0.32) \times 10^{-01}$				
HCN	12m	1-0	2010 Oct 28.3	$< 4.13 \times 10^{11}$	1.31×10^{-05}	$< 2.43 \times 10^{25}$	$< 3.81 \times 10^{-01}$				
			2010 Oct 23.54	$(7.95 \pm 1.75) \times 10^{11}$		$(1.32 \pm 0.29) \times 10^{25}$	$(1.95 \pm 0.44) \times 10^{-01}$				
			2010 Oct 22.53	$(3.35 \pm 1.10) \times 10^{11}$		$(9.32 \pm 3.10) \times 10^{24}$	$(1.37 \pm 0.45) \times 10^{-01}$				
			2010 Oct 21.48	$(8.28 \pm 0.55) \times 10^{11}$		$(6.23 \pm 0.42) \times 10^{24}$	$(9.19 \pm 0.72) \times 10^{-02}$				
HCN	JCMT	4-3	2010 Oct 22.43	$(8.73 \pm 1.44) \times 10^{11}$	1.31×10^{-05}	$(6.80 \pm 1.21) \times 10^{24}$	$(1.01 \pm 0.18) \times 10^{-01}$				
			2010 Oct 22.78	$(1.45 \pm 0.19) \times 10^{12}$		$(1.23 \pm 0.16) \times 10^{25}$	$(1.81 \pm 0.25) \times 10^{-01}$				
			2010 Oct 23.41	$(7.40 \pm 0.88) \times 10^{11}$		$(5.81 \pm 0.69) \times 10^{24}$	$(8.75 \pm 1.08) \times 10^{-02}$				
			2010 Oct 23.77	$(1.14 \pm 0.10) \times 10^{12}$		$(9.02 \pm 0.91) \times 10^{24}$	$(1.33 \pm 0.14) \times 10^{-01}$				
			2010 Nov 2.44	$(1.14 \pm 0.11) \times 10^{12}$		$(1.09 \pm 0.11) \times 10^{25}$	$(1.55 \pm 0.15) \times 10^{-01}$				
			2010 Nov 2.77	$(6.07 \pm 1.21) \times 10^{11}$		$(6.79 \pm 1.35) \times 10^{24}$	$(1.15 \pm 0.23) \times 10^{-01}$				
			2010 Nov 3.62	$(3.64 \pm 0.77) \times 10^{11}$		$(3.29 \pm 0.70) \times 10^{24}$	$(3.72 \pm 0.91) \times 10^{-02}$				
			2010 Nov 4.44*	$(7.40 \pm 1.21) \times 10^{11}$		$(8.07 \pm 1.32) \times 10^{24}$	$(9.13 \pm 1.87) \times 10^{-02}$				
			2010 Oct 25.56	$(5.36 \pm 1.15) \times 10^{11}$		$(5.78 \pm 1.24) \times 10^{24}$	$(8.53 \pm 1.86) \times 10^{-02}$				
			p-H ₂ CO	JCMT		5 _{0,5} - 4 _{0,4}	2010 Oct 21.56	$(1.14 \pm 0.26) \times 10^{11}$	2.15×10^{-04}	$(2.65 \pm 0.60) \times 10^{23}$	$(3.91 \pm 0.89) \times 10^{-03}$
							2010 Oct 23.57	$(2.41 \pm 1.05) \times 10^{11}$		$(1.02 \pm 0.43) \times 10^{24}$	$(1.50 \pm 0.53) \times 10^{-02}$
							2010 Nov 2.69	$(7.38 \pm 1.21) \times 10^{11}$		$(7.54 \pm 1.23) \times 10^{24}$	$(1.08 \pm 0.19) \times 10^{-01}$
			o-H ₂ CO	JCMT		5 _{1,5} - 4 _{1,4}	2010 Nov 2.58	$(5.21 \pm 1.19) \times 10^{11}$	1.31×10^{-05}	$(7.99 \pm 1.82) \times 10^{24}$	$(1.14 \pm 0.27) \times 10^{-02}$
							2010 Oct 22.58	$< 1.53 \times 10^{10}$		$< 1.36 \times 10^{23}$	$< 2.01 \times 10^{-03}$
DCN	JCMT	5-4	2010 Oct 23.57	$< 1.53 \times 10^{10}$	1.31×10^{-05}	$< 1.38 \times 10^{23}$	$< 2.04 \times 10^{-03}$				
			2010 Nov 2.69	$< 3.44 \times 10^{10}$		$< 3.77 \times 10^{23}$	$< 5.38 \times 10^{-03}$				
			2010 Nov 4.67*	$< 4.59 \times 10^{10}$		$< 5.27 \times 10^{23}$	$< 4.15 \times 10^{-03}$				
			2010 Nov 2.69	$< 3.09 \times 10^{10}$		$< 3.38 \times 10^{23}$	$< 4.82 \times 10^{-03}$				
HNC	JCMT	4-3	2010 Nov 4.67*	$< 4.33 \times 10^{10}$	1.31×10^{-05}	$< 5.08 \times 10^{23}$	$< 4.00 \times 10^{-03}$				

relationships between species in 103P as observed in the infrared: H₂CO depleted and HCN normal. Abundance ratios for other primary volatiles were obtained by Dello Russo et al. (2011) and Kawakita et al. (2013); they concluded that comet 103P is C₂H₂ normal, C₂H₆ normal, NH₃ normal, CH₃OH normal, CH₄ depleted and CO depleted.

4.3. D/H ratio

We used the JCMT data to compute an upper limit for the D/H ratio in HCN and DCN. Both species were sampled the same day. We average the gas production rate of DCN on UT 2010 October 22.58 and UT 2010 October 23.57 (Figure in Appendix D). The D/H ratios from HCN are given in Table 4. As discussed in section 4.2, we note variability of the HCN with time, and this short-term variability has been studied in detail by Boissier et al. (2014) and Drahus et al. (2012). We measured only upper limits for DCN, for which we assumed a constant HCN production rate over the period between the HCN and DCN observations on a given day.

Relevant deuterium fractionation ratios have been measured for both comets and the interstellar medium. Crovisier et al. (2004), Kawakita et al. (2005), Kawakita & Kobayashi (2009), Gibb et al. (2012) and Bonev et al. (2009) have presented upper limits for the production rates of several cometary molecules. D/H isotope ratios have been measured for two cometary molecules in 103P: water and hydrogen cyanide. Compared to models of interstellar chemistry, both the measured HDO/H₂O and DCN/HCN ratios are compatible with ion-molecule chemistry in gas at about 30-35 K. With this work we measured an upper limit for the DCN/HCN ratio of <0.01. Our value is consistent with previous measurements [e.g., D/H = 0.002 in comet Hale-Bopp; Meier et al. (1998), and 1.6×10^{-4} in comet 103P; Hartogh et al. (2011)], although it does not place any new constraints. By comparison, a range of (0.4 - 7.0) $\times 10^{-2}$ for the DCN/HCN ratio was determined in the interstellar medium (Roberts et al. 2002; Jørgensen et al. 2004).

4.4. OPR ratio from H₂CO

Molecules that contain multiple H atoms can be spectroscopically distinguished based on the

orientation of the spins of their H nuclei, either aligned in parallel or anti-parallel states (e.g. H₂, H₂CO, H₂O), giving rise to *ortho* and *para* forms. Quantum-mechanically, transitions between the different forms are strictly forbidden giving rise to two distinct spectra and *ortho* : *para* ratios (OPRs), which define the spin temperature (T_{spin}) of that species. This means that the relative abundances of nuclear spin isomers are expected to remain invariant over time, and the OPR has therefore been long thought to reveal information about the temperature of formation of cometary ices. However, some processes are hypothesized to change the OPR without breaking molecular bonds (e.g. Limbach et al. 2006), and phase transitions are effective in bringing the molecules into an equilibrated OPR (e.g. Hama & Watanabe 2013). In the study of water molecules trapped in low temperature (~ 4 K) solid Ar matrices, Sliter et al. (2011) found that upon desorption at $T > 260$ K, fast *ortho* – *para* conversion occurred. In addition, theoretical investigations (Anderson & van Dishoeck 2008) showed that photodesorption of water ice at 10 K would typically lead to bond breaking (with the subsequent loss of OPR information). Of the processes investigated by Anderson & van Dishoeck (2008), only the ‘kick-out’ mechanism would preserve the OPR during desorption at low temperatures. On the other hand, it is not straightforward to extrapolate the high-temperature desorption and Ar matrix-ice studies by Sliter et al. (2011) to the release of volatiles from cometary ices, and which process dominates the desorption of ices at low temperatures. The cosmogonic significance of OPR and spin temperature in comets is therefore not clear, and the lack of OPR measurements for molecules with smaller *ortho* – *para* energy deficiencies (e.g., H₂CO and CH₃OH) has further limited our understanding of this indicator in comets.

The OPR of H₂CO for Hartley 2 was obtained from consecutive observations of the *ortho*-H₂CO ($5_{0,5} - 4_{0,4}$) and *para*-H₂CO ($5_{1,5} - 4_{1,4}$) lines on November 2 from data obtained at the JCMT (see Table 1). The periodicity of the comet presents some uncertainty in abundances, though these two observations were in close enough proximity (< 3 hrs). Therefore, the variation in rotation temperature is likely not a major factor. Other obser-

Table 4: D/H ratio in comet 103P/Harley 2. We average Q_{DCN} on UT 2010 October 22.58-23.57.

UT Date	Q_{HCN} (s^{-1})	UT Date	Q_{DCN} (s^{-1})	D/H
2010 Oct 22.43	6.80×10^{24}	2010 Oct 22.58-23.57	$<1.37 \times 10^{23}$	$<2.01 \times 10^{-02}$
2010 Oct 22.78	1.23×10^{25}		$<1.37 \times 10^{23}$	$<1.11 \times 10^{-02}$
2010 Oct 23.41	5.81×10^{24}		$<1.37 \times 10^{23}$	$<2.36 \times 10^{-02}$
2010 Oct 23.77	9.02×10^{24}		$<1.37 \times 10^{23}$	$<1.52 \times 10^{-02}$
2010 Nov 2.44	1.09×10^{25}	2010 Nov 2.69	$<3.77 \times 10^{23}$	$<3.46 \times 10^{-02}$
2010 Nov 2.77	6.79×10^{24}	2010 Nov 2.69	$<3.77 \times 10^{23}$	$<5.55 \times 10^{-02}$
2010 Nov 4.44	8.07×10^{24}	2010 Nov 4.67	$<5.27 \times 10^{23}$	$<6.63 \times 10^{-02}$

vational uncertainties are factored out in the ratio. For these data we obtain an OPR $\approx 2.12 \pm 0.59$ (1σ), or $T_{\text{spin}} \approx 13.5_{-3.3}^{+6.7}$ K (1σ), although at only 1.5σ our OPR measurement cannot distinguish from equilibrium ($T_{\text{spin}} > 9$ K at 1.5σ). Similarly, Villanueva et al. (2012b) have measured $T_{\text{spin}} > 18$ K for CH_3OH in comet C/2001 A2 (LINEAR), which is consistent with that in Hale-Bopp $T_{\text{spin}} > 15$ K (Pardanaud et al. 2007). Our results are also consistent (within 1σ) with those obtained for water by Bonev et al. (2013) of OPR $\approx 2.79 \pm 0.13$ (mean of five measurements).

The complexity of obtaining simultaneous observations of *ortho* and *para*- H_2CO , and the difficulty in obtaining a good signal-to-noise ratio for these data enforces the future need for sensitive, broad-band telescope receivers where these can be readily measured towards any comet. Such measurements will provide the necessary context to better understand the cosmogonic significance (or lack of) of our OPR measurement of $\approx 2.12 \pm 0.59$ (1σ).

5. Comparison among various comets

Knowledge of the volatile chemistry of Jupiter-Family comets (Kuiper Belt) is very limited from both infrared and radio observations because Jupiter-Family comets have typically lower activity.

Crovisier et al. (2009) show the compositional diversity among Jupiter-Family comets from radio observations. Before the observation of 103P, about a dozen Jupiter-Family comets have been observed by radio techniques. By comparing the relative abundance of HCN among Jupiter-Family comets, Crovisier et al. (2009) reported that 2P/Encke, 9P/Tempel 1 and 22P/Kopff are organics-normal, like 103P, while 19P/Borrelly, 21P/Giacobini-Zinner and 73P/Schwassmann-

Wachmann 3 are organics-depleted. This suggests distinct processing histories for organics-depleted, organics-normal and organics-enriched comets. Dello Russo et al. (2011) and Kawakita et al. (2013) compared the abundances ratios among Jupiter-family sampled from infrared observations. The limited sample of few Jupiter-Family comets shows again that diversity is notable. For example, Dello Russo et al. (2011) concluded that 73P/Schwassmann-Wachmann 3 and 103P are extremely different in their chemical composition.

Correlations between short-term temporal variations in production rates of primary volatiles with nucleus rotation have been suggested only for two Oort cloud comets. Biver et al. (2009) reported a periodic variation of 40% in the water production rate in C/2001 Q4 (NEAT), with a period of 19.58 ± 0.1 hrs. Anderson (2010) observed a variation in production rates for H_2O , CO , H_2CO , and CH_3OH in comet C/2002 T7 (LINEAR) with a period of 2.32 days. Comet 103P is the third comet for which periodic variation in production of primary volatiles has been demonstrated, and the first one for which unambiguous association with nucleus rotation can be made through imaging (A'Hearn et al. 2011; Harmon et al. 2010, 2011).

To date, OPRs have been measured in a few species, namely NH_3 , H_2O , and CH_4 , for several comets by ground-based observations (see Bockelée-Morvan et al. 2004; Dello Russo et al. 2005; Kawakita & Watanabe 2002; Kawakita et al. 2001; Mumma et al. 2011). Dello Russo et al. (2005) reported from H_2O , $T_{\text{spin}} > 30$ K, $T_{\text{spin}} = 30_{-6}^{+15}$ K, $T_{\text{spin}} = 23_{-3}^{+4}$ K respectively in comets C/1999 H1 (Lee), C/1999 S4 (LINEAR), and C/2001 A2 (LINEAR). Kawakita et al. (2001) and Kawakita & Watanabe (2002) derived an OPR of ammonia equal to 1.17 ± 0.04 and 1.12 ± 0.03 (or $T_{\text{spin}} = 30_{-2}^{+3}$ K) respectively in comet C/1999 S4 (LINEAR) and C/2001 A2 (LINEAR). Some of

the OPR ratios imply formation temperatures for cometary ice species of 25 – 35 K, similar to the formation temperature implied by the D/H ratios in H₂O and HCN, but a growing sample of comets also show equilibrated OPR ($T_{spin} > 35$ K, e.g. Villanueva et al. 2012a; Mumma et al. 1993). For example, Mumma et al. (1993) reported a water OPR = 3.2 ± 0.2 for C/1986 P1 (Wilson) ($T_{spin} > 50$ K).

6. Conclusions

We conducted observations of comet 103P/Hartley 2 at both perihelion and at the time of the EPOXI flyby. We report detections of HCN, H₂CO, CS, and OH and upper limits of HNC and DCN, using the ARO Kitt Peak 12m and SMT, JCMT and the GBT towards comet 103P. We derived column densities, production rates, and relative abundances toward comet 103P. We concluded that 103P is normal in HCN and depleted in H₂CO which is in good agreement with other studies. We obtained an upper limit the (D/H)_{HCN} ratio of < 0.01 and an *ortho* : *para* ratio of 2.2 ± 0.59 (1σ) has been derived from H₂CO.

Acknowledgements:

The National Radio Astronomy Observatory is a facility of the National Science Foundation operated under cooperative agreement by Associated Universities, Inc. The Kitt Peak 12m telescope and the Submillimeter telescope are currently operated by the Arizona Observatory (ARO), Steward Observatory, University of Arizona, with partial funding from the Research Corporation. The James Clerk Maxwell Telescope is operated by the Joint Astronomy Centre on behalf of the Science and Technology Facilities Council of the United Kingdom, the Netherlands Organisation for Scientific Research, and the National Research Council of Canada. This work was supported by the Goddard Center for Astrobiology, by NASA’s Planetary Astronomy and Planetary Atmospheres Programs. YJK acknowledges support from NSC grants 100-2119-M-003-001-MY3 and 102-2119-M-003-008- for this work.

REFERENCES

A’Hearn, M. F., Millis, R. L., Schleicher, D. G., et al. 1995, *Icarus*, 118, 223

A’Hearn, M. F., Belton, M. J. S., Delamere, W. A., et al. 2005, *Science*, 310, 258

A’Hearn, M. F., Belton, M. J. S., Delamere, W. A., et al. 2011, *Science*, 332, 1396

Anderson, H. & von Dishoeck, E. F. 2008, *A&A*, 491, 907

Anderson, Jr., W. M. 2010, in PhD thesis, The Catholic University of America

Bast, J. E., Lahuis, F., van Dishoeck, E. F., et al. 2013, *A&A*, 551, A118

Biver, N., Bockelée-Morvan, D., Crovisier, J., et al. 2007, *P&SS*, 55, 1058

Biver, N., Bockelée-Morvan, D., Colom, P., et al. 2009, *A&A*, 501, 359

Biver, N., Bockel’Ee-Morvan, D., Crovisier, J., et al. 2011, EPSC-DPS Joint Meeting 2011, 938

Bockelée-Morvan, D., Crovisier, J., Mumma, et al. 2004, in *Comets II*, ed M. C. Festou, H. U. Keller, and H. A. Weaver (Tucson, AZ: University of Arizona Press), 391

Bockelée-Morvan, D. & de Bergh, C. 2005, *P&SS*, 53, 1203

Boissier, J., Bockelée-Morvan, D., Biver, N., et al. 2014, *Icarus*, 228, 197

Bonev, B. P., Mumma, M. J., Gibb, E. L., et al. 2009, *ApJ*, 699, 1563

Bonev, B. P., Villanueva, G. L., Paganini, L., et al. 2013, *Icarus*, 222, 740

Brownlee, D., Tsou, P., Aléon, J., et al. 2006, *Science*, 314, 1711

Chyba, C. F., Thomas, P. J., Brookshaw, L., et al. 1990, *Science*, 249, 366

Clemett, S. J., Sandford, S. A., Nakamura-Messenger, K., et al. 2010, *Meteoritics and Planetary Science*, 45, 701

Combi, M. R., Bertaux, J.-L., Quémerais, E., et al. 2011, *ApJL*, 734, L6

Colangeli, L., Epifani, E., Brucato, J. R., et al. 1999, *A&A*, 343, 87

- Crovisier, J., Leech, K., Bockelee-Morvan, D., et al. 1997, *Science*, 275, 1904
- Crovisier, J., Encrenaz, T., Lellouch, E., et al. 1999, *The Universe as Seen by ISO*, ed. P. Cox & M. F. Kessler (ESA-SP), 427, 161
- Crovisier, J., Bockelée-Morvan, D., Colom, P., et al. 2004, *A&A*, 418, 1141
- Crovisier, J., Biver, N., Bockelée-Morvan, D., et al. 2009, *P&SS*, 57, 1162
- Crovisier, J., Colom, P., Biver, N., et al. 2013, *Icarus*, 222, 679
- Dello Russo, N., Bonev, B. P., DiSanti, et al. 2005, *ApJ*, 621, 537
- Dello Russo, N., Vervack, Jr., R. J., Lisse, C. M., et al. 2011, *ApJL*, 734, L8
- Dello Russo, N., Vervack, R. J., Weaver, H. A., et al. 2013, *Icarus*, 222, 707
- Dickens, J. E. & Irvine, W. M. 1999, *ApJ*, 518, 733
- Duncan, M., Levison, H., and Dones, L. 2004, in *Comets II*, ed M. C. Festou, H. U. Keller, and H. A. Weaver (Tucson, AZ: University of Arizona Press), 193
- Dodson-Robinson, S. E., Willacy, K., Bodenheimer, P., et al. 2009, *Icarus*, 200, 672
- Drahus, M., Jewitt, D., Guilbert-Lepoutre, A., et al. 2012, *ApJ*, 756, 80
- Feldman, P. D., Cochran, A. L., and Combi, M. R. 2005, in *Comets II*, ed M. C. Festou, H. U. Keller, and H. A. Weaver (Tucson, AZ: University of Arizona Press), 425
- Festou, M. C., Keller, H. U., and Weaver, H. A. 2004, in *Comets II*, ed M. C. Festou, H. U. Keller, and H. A. Weaver (Tucson, AZ: University of Arizona Press), 3
- Fink, U. 2009, *Icarus*, 201, 311
- Gibb, E. L., Bonev, B. P., Villanueva, G., et al. 2012, *ApJ*, 750, 102
- Hama, T. & Watanabe, N. 2013, *ChRv*, 113, 8783
- Harmon, J. K., Nolan, M. C., Howell, E. S., et al. 2010, *IAU Circ.*, 9179, 1
- Harmon, J. K., Nolan, M. C., Howell, E. S., et al. 2011, *ApJL*, 734, L2
- Harris, W. M., Scherb, F., Mierkiewicz, E., et al. 2002, *ApJ*, 578, 996
- Hartley, M. 1986, *IAU Circ.* 4197, 1
- Hartogh, P., Lis, D. C., Bockelée-Morvan, D., et al. 2011, *Nature*, 478, 218
- Haser, L. 1957, in *Bulletin de la Class des Sciences de l'Académie Royale de Belgique*, 43, 740
- Hines, D. C., Videen, G., Zubko, E., et al. 2014, *ApJL*, 780, L32
- Huebner, W. F., Keady, J. J., and Lyon, S. P. 1992, *Ap&SS*, 1995, 289
- Jørgensen, J. K., Schöier, F. L., and van Dishoeck, E. F. 2004, *A&A*, 416, 603
- Kawakita, H., Watanabe, J.-i., Ando, H. et al. 2001, *Science*, 294, 1089
- Kawakita, H. & Watanabe, J. 2002, 34th COSPAR Scientific Assembly, 34
- Kawakita, H., Watanabe, J.-i., Furusho, R., et al. 2005, *ApJL*, 623, L49
- Kawakita, H. & Kobayashi, H. 2009, *ApJL*, 693, 388
- Kawakita, H., Kobayashi, H., Dello Russo, N., et al. 2013, *Icarus*, 222, 723
- Knight, M. M., Walsh, K. J., A'Hearn, M. F., et al. 2007, *Icarus*, 187, 199
- Knight, M. M. & Schleicher, D. G. 2012, *Icarus*, 222, 691
- Levison, H. F. & Duncan, M. J. 1997, *Icarus*, 127, 13
- Levison, H. F., Dones, L., and Duncan, M. J. 2001, *AJ*, 121, 2253
- Limbach, H.-H., Buntkowsky, G., Matthes, J., et al. 2006, *Physical Chemistry Chemical Physics*, 7, 551

- Lis, D. C., Bockelee-Morvan, D., Biver, N., et al. 2010, IAU Circ. 9185
- Lisse, C. M., Fernandez, Y. R., Reach, W. T., et al. 2009, Publications of the Astronomical Society of the Pacific, 121, 968
- McKeegan, K. J., Aléon, J., Bradley, J. et al. 2006, Science, 314, 1724
- Meech, K. J., Ageorges, N., A'Hearn, M. F., et al. 2005, Science, 310, 265
- Meech, K. J., A'Hearn, M. F., Adams, J. A., et al. 2011, ApJL, 734, L1
- Meier, R., Owen, T. C., Jewitt, D. C., et al. 1998, Science, 279, 1707
- Milam, S. N., Savage, C., Ziurys, L. M., et al. 2004, ApJ, 615, 1054
- Milam, S. N., Remijan, A. J., Womack, M., et al. 2006, ApJ, 649, 1169
- Mumma, M. J., Weissman, P. R., and Stern, S. A. 1993, in Protostars and Planets III, 1177
- Mumma, M. J., Bonev, B. P., Villanueva, G. L., et al. 2011, ApJL, 734, L7
- Mumma, M. J. & Charnley, S. B. 2011, Annual Review of Astronomy and Astrophysics, 49, 471
- Newburn, Jr., R. L., Neugebauer, M., and Rahe, J. 1991, IAU Colloq. 116: Comets in the post-Halley era, 167
- Pardanaud, C., Crovisier, J., Bockelée-Morvan, D., et al. 2007, SF2A-2007: Proceedings of the Annual meeting of the French Society of Astronomy and Astrophysics, 421
- Roberts, H., Fuller, G. A., Millar, T. J., et al. 2002, P&SS, 50, 1173
- Reach, W. T., Kelley, M. S., and Vaubaillon, J. 2013, Icarus, 226, 777
- Schleicher, D. G., A'Hearn, M. F. 1988, ApJ, 331, 1058
- Schulz, R. 2012, P&SS, 66, 1
- Sliter, R., Gish, M., and Vilesov, A. F. 2011, JPhCh, 115, 9682
- Starkey, N. A. & Franchi, I. A. 2013, Geochimica et Cosmochimica Acta, 105, 73
- Tacconi-Garman, L. E., Schloerb, F. P., and Claussen, M. J. 1990, ApJ, 364, 672
- Ulich, B. L. & Haas, R. W. 1976, Astrophysical, Suppl. Ser., 30, 247
- Villanueva, G. L., Mumma, M. J., Bonev, B. P., et al. 2012a, JQSRT, 113,202
- Villanueva, G. L., DiSanti, M. A. Mumma, M. J., et al. 2012b, ApJL, 747,37
- Villanueva, G. L., Magee-Sauer, K., Mumma, M. J., et al. 2013, JQSRT 129,158

This 2-column preprint was prepared with the AAS L^AT_EX macros v5.2.

A. Detection of OH

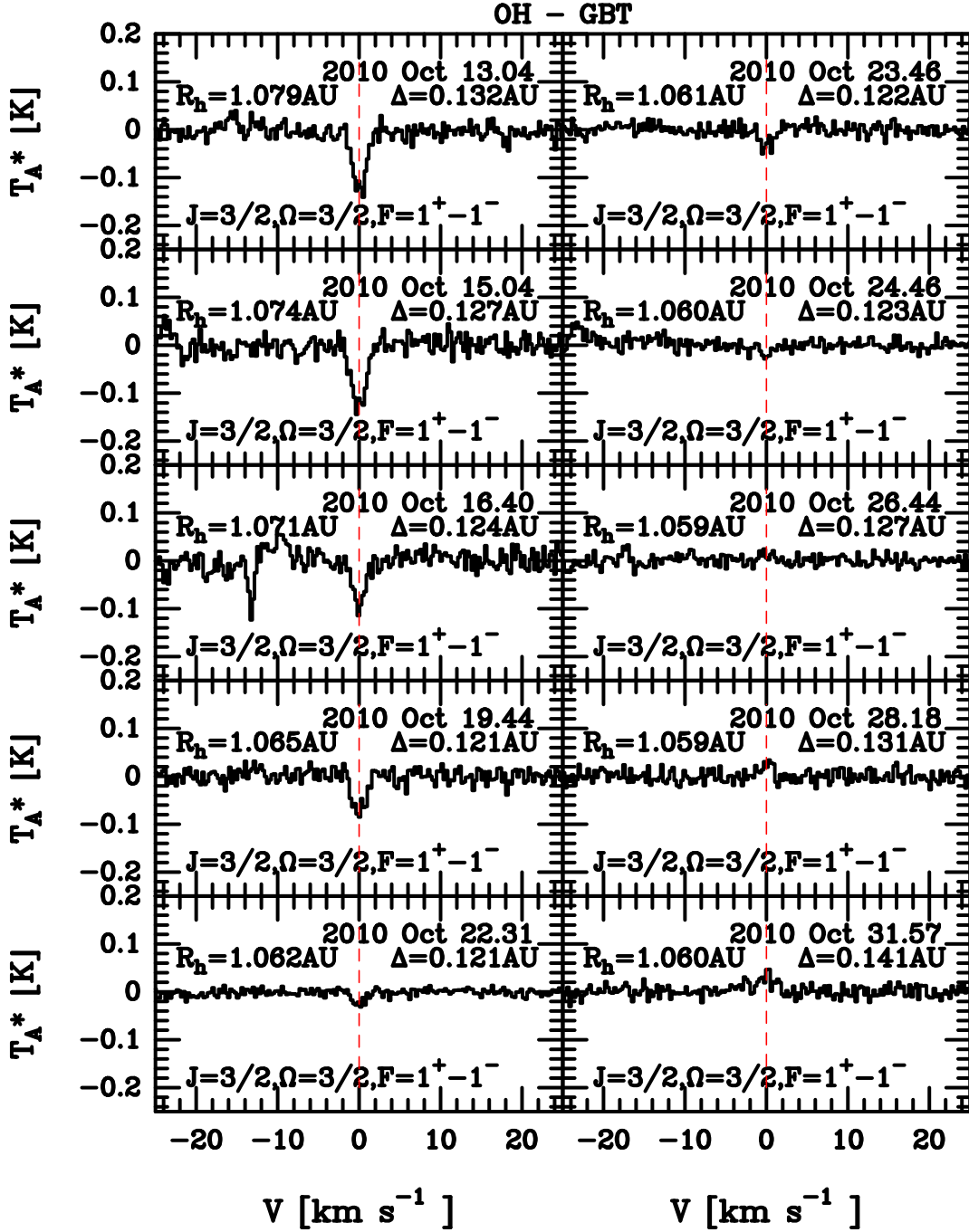


Fig. 6.— Detection and upper limit of OH taken for each day of the observations with the GBT. The spectral resolution is $\approx 0.274 \text{ km s}^{-1}$. Spectra are plotted in a cometocentric velocity frame. The red-dashed line denotes the $J=3/2, \Omega=3/2, F=1^+-1^-$ transition at the comet velocity. Other features present in spectra are attributed to interstellar features at the time of observations.

B. Detection of HCN

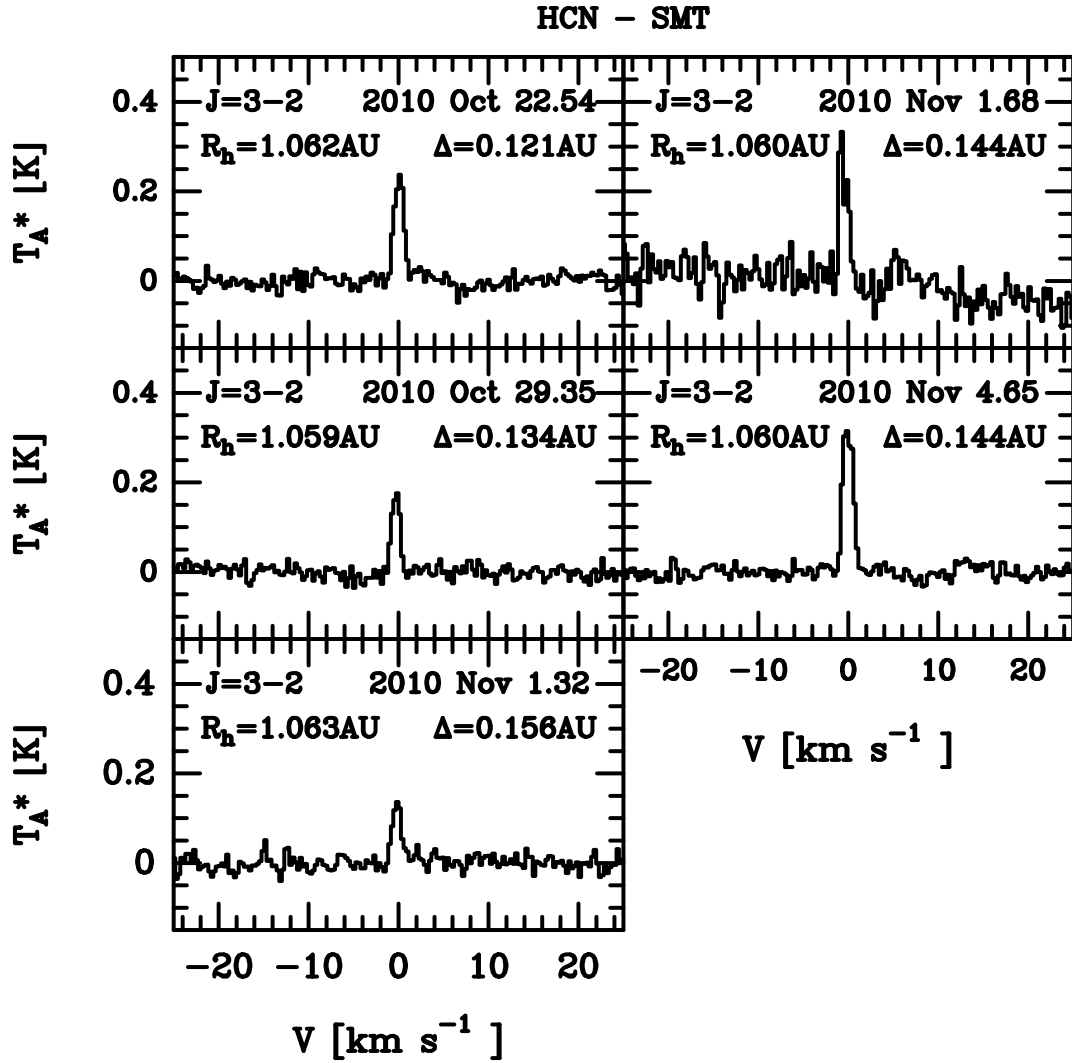


Fig. 7.— Detection of HCN 3-2 taken for each day of observations with the SMT. The spectral resolution is ≈ 0.280 km s⁻¹. Spectra are plotted in a cometocentric velocity frame.

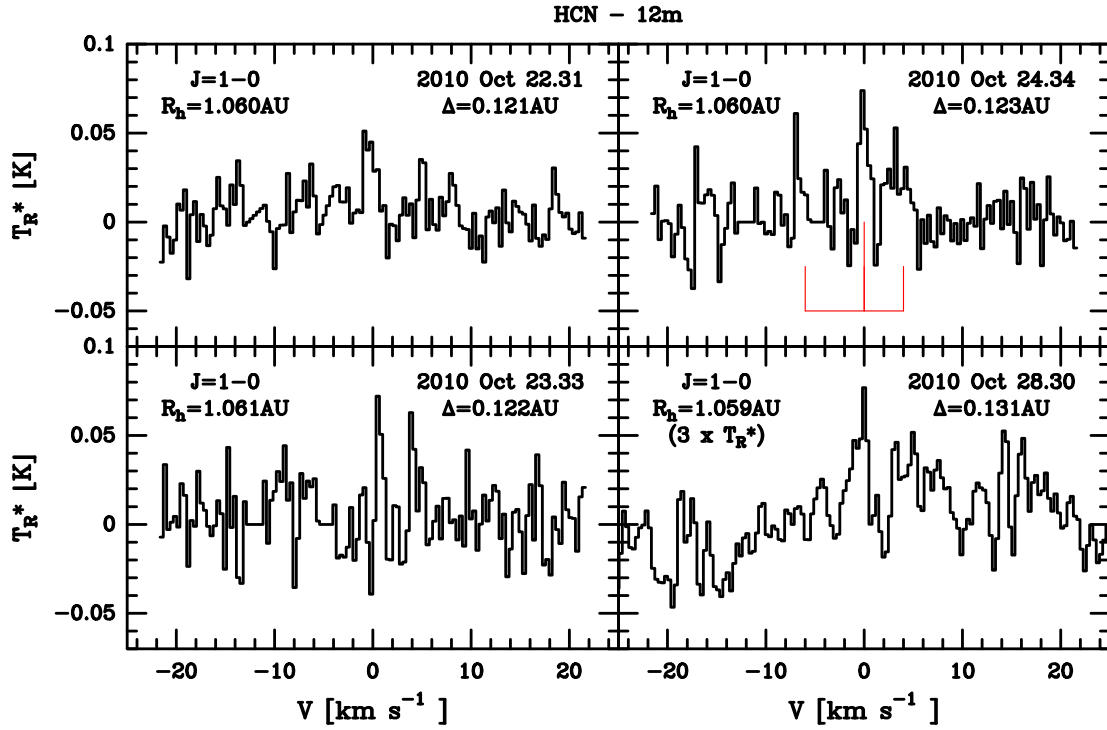


Fig. 8.— Detection of HCN 1-0 for each day of observation with the 12m. The spectral resolution is ≈ 0.340 km s^{-1} . Spectra are plotted in a cometocentric velocity frame. Relative intensities of the hyperfine lines are plotted below on 2010 Oct. 24.34. T_R^* was multiplied by a factor 3 on Oct. 28.30.

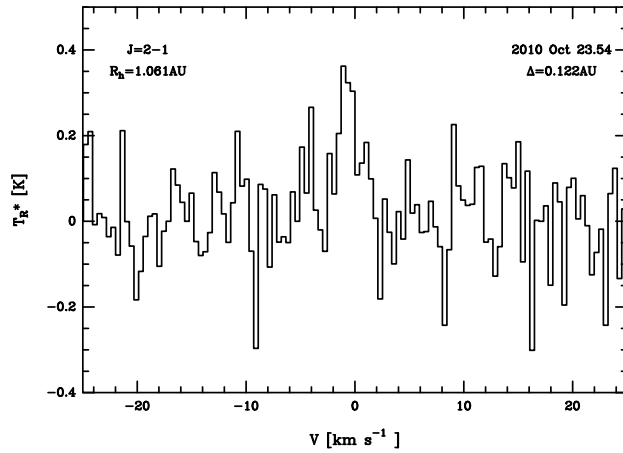


Fig. 9.— Detection of HCN 2-1 taken on 23 October 2010 with the 12m. The spectral resolution is ≈ 0.170 km s^{-1} . Spectra is plotted in a cometocentric velocity frame.

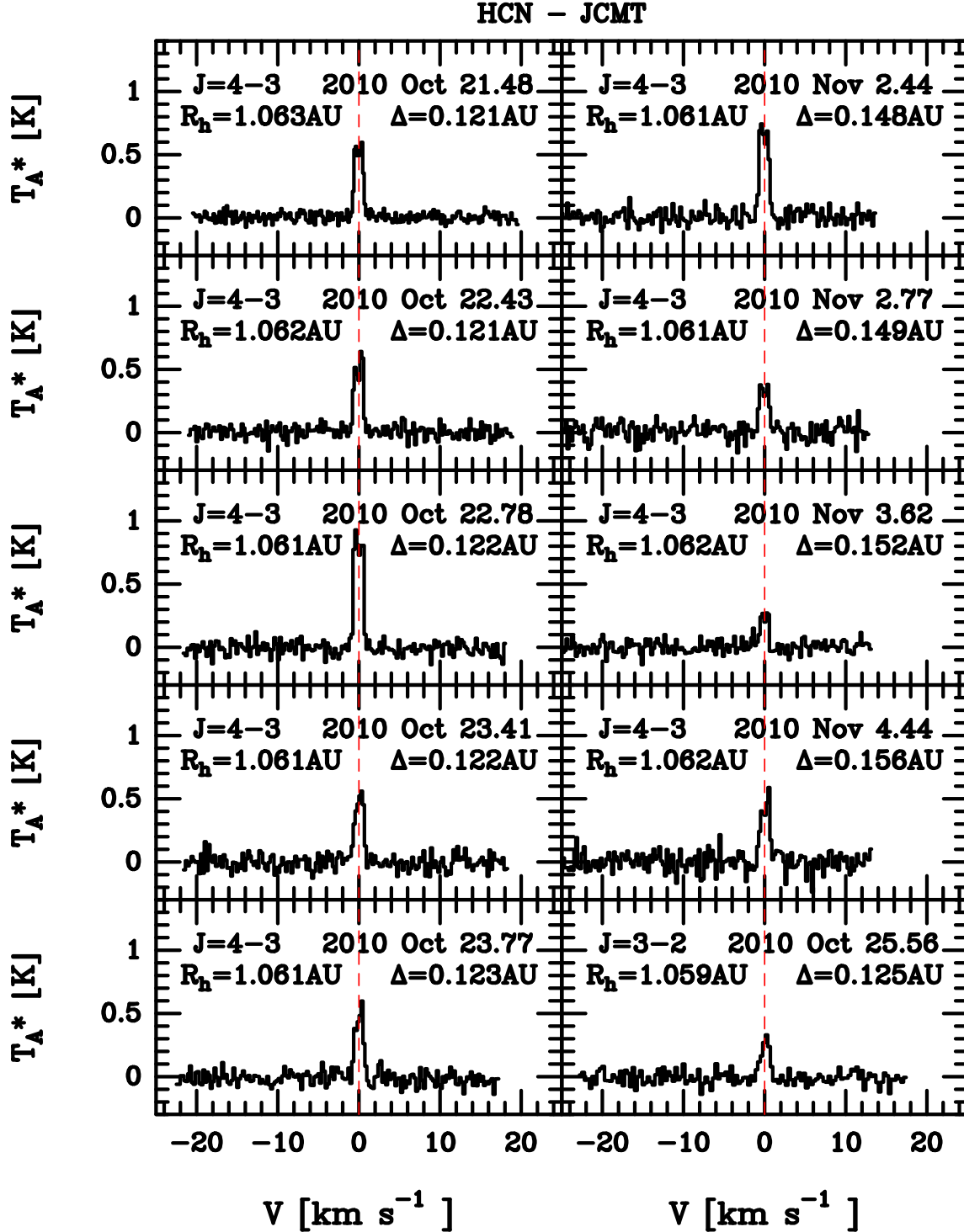


Fig. 10.— Detection of HCN 4-3 and 3-2 taken for each day of observations with the JCMT. The spectral resolution are $\approx 0.232 \text{ km s}^{-1}$ and $\approx 0.310 \text{ km s}^{-1}$ for the 4-3 and 3-2 transition, respectively. Spectra is plotted in a cometocentric velocity frame. The observed asymmetry in the line profile observed can be attributed to localized outgassing as mentioned by Kawakita et al. (2013)

C. Detection of H₂CO

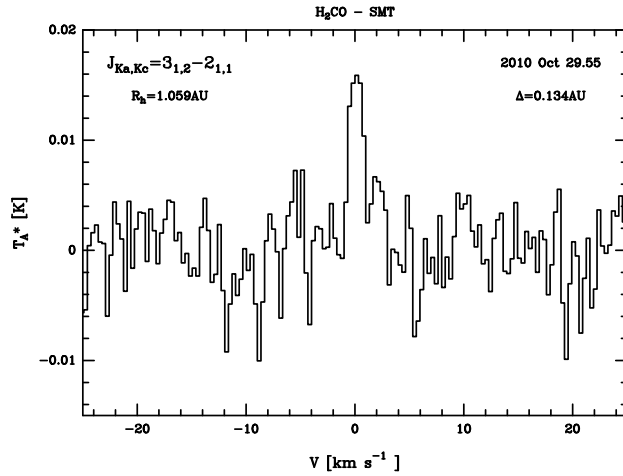


Fig. 11.— Detection of H₂CO taken on 29 October 2010 with the SMT. The spectral resolution is ≈ 0.332 km s⁻¹. Spectra are plotted in a cometocentric velocity frame.

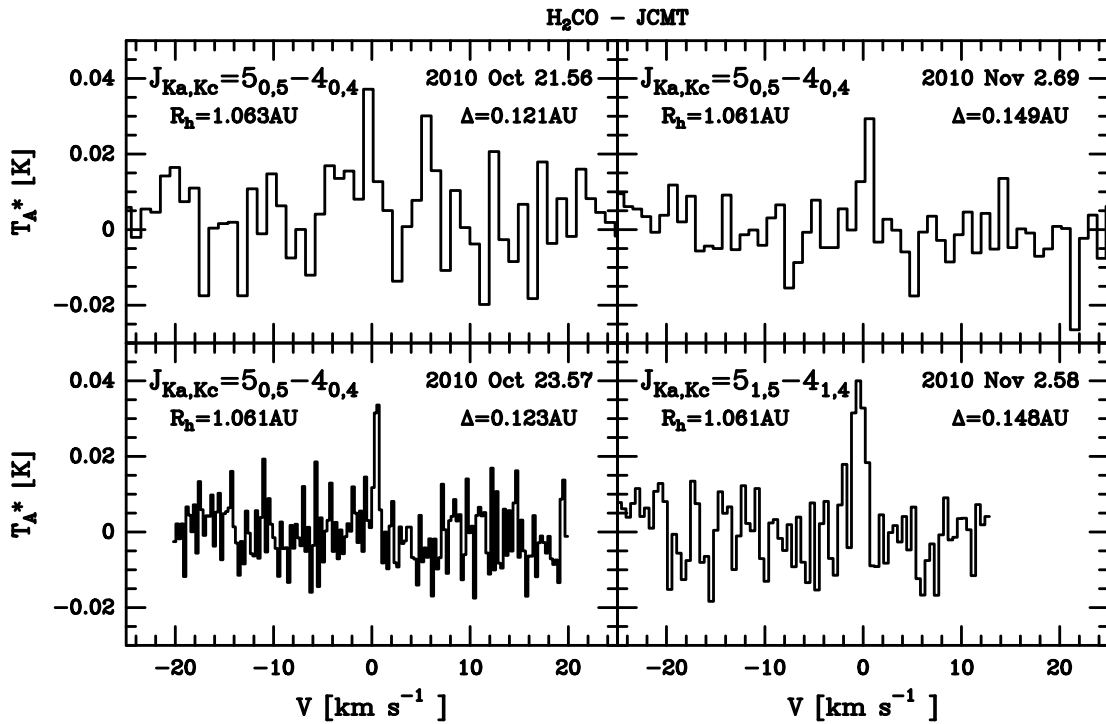


Fig. 12.— Detection of H₂CO taken for each day of observations with the JCMT. The spectral resolution are ≈ 0.984 km s⁻¹, ≈ 0.252 km s⁻¹, ≈ 0.909 km s⁻¹ and ≈ 0.468 km s⁻¹ on 21 October, 23 October, 2.69 November and 2.58 November, respectively. Spectra are plotted in a cometocentric velocity frame.

D. Detection of HCN and upper limit of DCN

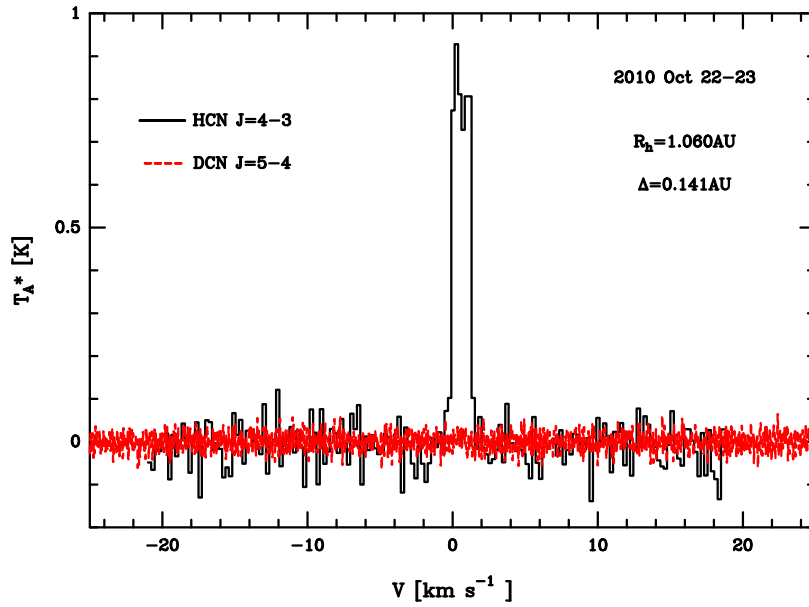


Fig. 13.— Detection of HCN on taken on 22 October 2010 and average for the upper limit of DCN taken on 22-23 October 2010 with the JCMT. The spectral resolution are $\approx 0.232 \text{ km s}^{-1}$ and $\approx 0.025 \text{ km s}^{-1}$ for HCN and DCN, respectively. Spectra are plotted in a cometocentric velocity frame. The D/H ratio obtained here is < 0.01